Proceedings of the 17th World Congress
The International Federation of Automatic Control
Seoul, Korea, July 6-11, 2008

An Aerostat Positioning System with Cable Control

Casey Lambert * **Meyer Nahon** **

* *Department of Aeronautics and Astronautics, Tokyo University, Tokyo, Japan (e-mail: clambert@space.t.u-tokyo.ac.jp).*
** *Department of Mechanical Engineering, McGill University, Montreal, Quebec, Canada (e-mail: meyer.nahon@mcgill.ca).*

Abstract: The capabilities of a tri-tethered aerostat positioning system are investigated using simulations of a comprehensively validated dynamics model. The physical system studied consists of a payload supported by a helium filled aerostat and attached to three anchored ground tethers actuated using winches. Closed-loop control is achieved by feeding back the position of a payload located at the confluence point of the tethers. The dynamics model of the system is used to simulate the behavior of the closed-loop system. In a comparison of PID and optimal LQG control, a 50% improvement is achieved with the LQG controller. Both the LQG and PID feedback controllers were shown to benefit considerably from the addition of a feedforward control term that exploits measurements of the system's main disturbance force.

1. INTRODUCTION

Tethered aerostats are commonly used for hoisting aerial communication, surveillance and atmospheric sensing platforms. Typically, these systems use only a single cable to tether the aerostat to the ground. The precision of the tethered aerostat's station-keeping abilities can be greatly enhanced by attaching the platform to a series of tethers fixed to the ground in a spatial arrangement, Leclaire and Rice [1973], Nahon [1999]. When three tethers with equidistant terminations are used, the tethers form a tripod, which upon loading from the lifting force of the aerostat, form a light-weight tension structure as shown in Figure 1. Additionally, the tethers may be actuated on the ground to enhance the system's stability further and to guide the payload along a specified path, Nahon et al. [2002]. This work presents a study of the controlled disturbance-rejection capabilities of this type of tri-tethered aerostat system. Simulations of a previously developed and validated dynamics model are used to compare controllers that use proportional, integral, and derivative (PID) and optimal feedback alone and with a feedforward component.

Early experimental investigations of a tri-tethered aerostat system with fixed tether lengths were performed for the US Air Force, Leclaire and Rice [1973], and by Russian meteorologists, Masterskikh [1978]. Recently, astronomers in France performed tests on an actuated aerostat system consisting of six tethers in a double-tripod arrangement for a proposed optical telescope, Coroller et al. [2004]. Although no quantitative results for the motion of the payload were presented, the concept proved feasible as astronomical observations were recorded.

⋆ This work was supported in part by Canada's Natural Science and Engineering Research Council and Canada's National Research Council.

The multi-tethered aerostat system of the current work may be viewed as a large-scale cable-driven robotic manipulator, similar to other systems that have been studied previously. Starting with *Robocrane* in the early 1990s, Albus et al. [1993], a new class of parallel manipulators has emerged that employ cable actuators instead of traditional rigid members. The tri-tethered aerostat, which is essentially a 3-degree of freedom parallel manipulator, differs from conventional cable manipulators as it is inverted, relying on buoyancy to tension the tethers instead of gravity. Significant research has been conducted into the kinematics, dynamics and control of cable manipulators, Roberts et al. [1998], Kossowski and Notash [2002], Oh et al. [2005], Barrette and Gosselin [2005], however, the size of their workspace is generally limited to several meters which is about two orders of magnitude less than our tethered system. Due to the drastic difference in the length of the cables, which are the primary actuators, the modeling and experimental analysis techniques of the smaller mechanisms do not include all the important cable dynamics that affect the much larger aerial positioning system.

Researchers in China have studied a cable manipulator that is at a similar scale to our system, Duan [1999], which is designed as a receiver positioning device for a large radio telescope. The main difference of the Chinese concept is that instead of using an aerostat for lift, its receiver is suspended from multiple cables extending radially to tall tower supports. A fuzzy controller was developed to control cable length, Su et al. [2005], however, the cables were modeled as a pure time delay, which is an oversimplicification that ignores known cable oscillatory modes and performance variability due to loading.

Theoretical studies of a multi-tethered aerostat system involving discretized tethers that overcome the limitations of simple cable models, were initiated for a tri-tethered system with a spherical aerostat, Nahon [1999]. Unlike all

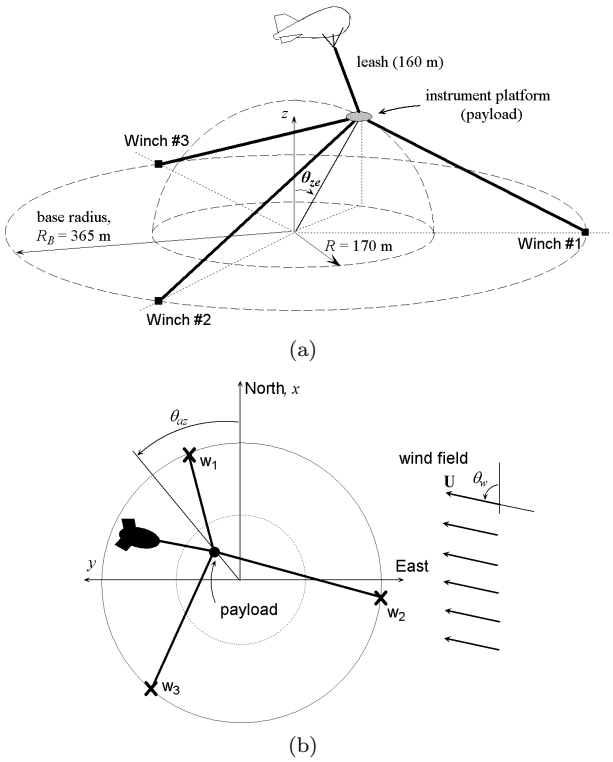

Fig. 1. a) Schematic diagram of proposed tri-tethered aerostat positioning system, b) overhead view.

previous studies of multi-tethered aerostat systems which assume passive tethers, an analysis was presented using actuated tethers with a PID feedback control scheme. Simulation results predicted that the station keeping performance of the aerostat positioning system could be drastically improved using basic feedback control. This study was expanded to include a comprehensive model of a streamlined aerostat and to investigate slewing maneuvers, Nahon et al. [2002]. To corroborate the simulation results with experimental data, a tri-tethered aerostat position system was constructed at the Dominion Radio Astrophysical Observatory (DRAO) in Penticton, B.C., Lambert et al. [2003]. The dynamics model of the aerostat positioning system was shown to agree favorably with experimental results without control, Lambert et al. [2006a], and with control, Lambert et al. [2006b].

The proposed aerostat system, shown schematically in Figure 1, was based on the conceptual design for a novel radio telescope termed the Large Adaptive Reflector (LAR), Fitzsimmons et al. [2000]. The LAR concept uses a tethered aerostat system to position a receiver during operation of the radio telescope. During telescope operation the antenna/feed package housed at the confluence point of the tethers must be positioned at points on a hemisphere down to a zenith angle, θ_{ze}, of 60° as shown in Figure 1. The tracking of the desired position and a certain level of disturbance rejection can be realized by actively adjusting the lengths of the ground tethers using winches operating under closed-loop control. The current study involves only three actuated tethers as only the position of the confluence point is to be controlled, but future efforts will likely involve at least six tethers to achieve some level of orientation control.

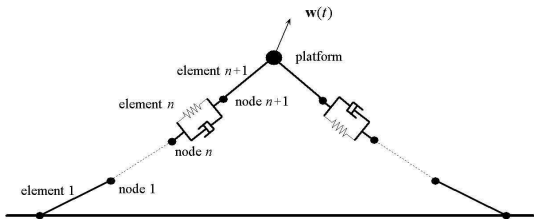

Fig. 2. 2-D representation of discretized dynamics model with one tether element expanded to show visco-elastic elements.

2. DYNAMICS MODEL

A dynamics model of the tethered aerostat system was developed to simulate the behavior of the system, Nahon [1999], Nahon et al. [2002]. The dynamics model is achieved by discretizing the system into a series of interconnected lumped masses. The tethers are split into nodes or lumped-masses connected by visco-elastic elements as shown in Figure 2. The strength of this tether model is its relatively simple numerical implementation and its ability to accurately represent long cables whose profiles and dynamics behavior change with loading, Driscoll et al. [2000], Lambert et al. [2006a]. The mass of each tether element is equally distributed to its two connected nodes and the internal forces or tension, T applied to the each node is based on the following linear relationships with the strain, ε and strain rate $\dot{\varepsilon}$ of each element:

$$T_i = AE\varepsilon + b\dot{\varepsilon}, \quad \varepsilon = \frac{L_i - L_0}{L_0} \tag{1}$$

where L^i and L_0 are the stretched and unstretched length of the i-th element, A is its cross sectional area, E is the effective Young's modulus of the cable, and b is the viscous damping coefficient of the cable. The stiffness of each tether element, k_i is related to Young's modulus using $k_i = EA/L_0$.

The model shown in Figure 2 does not contain the aerostat, which is instead represented by an experimentally obtained forcing function, $\mathbf{w}(t)$, applied to the platform. This simplified approach reduces the uncertainty with modeling the aerostat's aerodynamics by applying the force developed in the aerostat's leash during actual flight tests. When a controller is active, this approach neglects any aerostat dynamics induced by the control input, but the magnitude of the control input is much smaller than the wind induced forcing input. The magnitude of the leash force was measured using an inline load cell and its direction was estimated using GPS measurements of the aerostat and the platform.

The tether actuation system (performed by ground winches with the experimental system, Lambert et al. [2006b]) is incorporated with the dynamics model by actively adjusting the length of the bottom most tether element according to the desired controller output, $\dot{L}_i$. This discrete step change to the tether length approximates the continuous length change achieved by the real winching system. Typically, the iteration time step of the simulation is 1 ms or less, which provides a smooth response and small length changes. Also included in the overall dynamics is a second-order model for the winch actuators whose parameters were estimated using test data, Lambert [2006].

2.1 Linear Model

The original dynamics model is nonlinear, Nahon [1999], Nahon et al. [2002], but for the purposes of controller development, a linear model was obtained using a numerical finite difference technique. The linear time invariant (LTI) model of the system in state-space form is as follows:

$$\begin{aligned} \dot{\mathbf{x}} &= \mathbf{A}\mathbf{x} + \mathbf{B}\mathbf{u} + \mathbf{G}\mathbf{w} \\ \mathbf{y} &= \mathbf{C}\mathbf{x} \end{aligned} \tag{2}$$

where $\mathbf{x}$ is the state vector, which includes the velocities and positions of each discretized node, starting at the bottom of tether 1 up to the platform node, $\mathbf{x} = [\dot{x}_1\ x_1\ \dot{y}_1\ y_1\ \dot{z}_1\ z_1 ... \dot{x}_p\ x_p\ \dot{y}_p\ y_p\ \dot{z}_p\ z_p]^T$; $\mathbf{u}$ is the control input vector, which includes the three tether velocities, $\mathbf{u} = [\dot{L}_1\ \dot{L}_2\ \dot{L}_3]^T$; $\mathbf{w}$ is the disturbance force applied to the platform; and $\mathbf{y}$ is the output, which contains the position vector of the instrument platform $\mathbf{y} = [x_p\ y_p\ z_p]^T$.

The state matrix, $\mathbf{A}$, and the control matrix, $\mathbf{B}$, are obtained numerically while the input matrix, $\mathbf{G}$, and the output matrix, $\mathbf{C}$, are obtained intuitively. Typically, the tethers are discretized into 10 elements each which leads to 168 state variables (6×28 nodes–nine nodes for each of the three tethers and one for the platform). The nonlinear model contains additional state vector for the leash and aerostat nodes above the platform, but because the leash force is applied as the disturbance, all nodes above the platform are disregarded.

It was observed during the model validation process that nearly all the platform deflections during tests resulted directly from the disturbance force applied by the aerostat's leash, Lambert et al. [2006a]. Therefore, to apply a realistic disturbance to the linear model, the measured leash tension, resolved into Cartesian coordinates is used as $\mathbf{w}(t)$. To apply $\mathbf{w}$ directly to the equations of motion of the platform, the matrix $\mathbf{G}$ has three non-zero terms corresponding to the platform's velocity state variables, i.e. $G_{163,1} = G_{165,2} = G_{167,3} = 1/m_p$, where $m_p = 17.9$ kg is the mass of the platform.

To determine the fidelity of the linear model, a comparison of linear and nonlinear simulation results are presented in Figure 3. Matlab's Simulink is used to simulate the response of the LTI system. The disturbance $\mathbf{w}(t)$ was obtained from a flight on May 27, 2005. This case was chosen because of its high wind speed (≈ 4 m/s) relative to the other closed-loop flights. The results in Figure 3 are for an uncontrolled case in the symmetric configuration ($\theta_{ze} = 0°$). The plots show that the linear model slightly underestimates the motion in the horizontal directions while slightly overestimating the motion vertically. The discrepancies in the linear results may be attributed to the omission of certain nonlinear effects such as aerodynamic drag; however, the difference between the two sets of results is not significant enough to discourage usage of this linear model to develop and test controllers.

3. CONTROL SYSTEM

The control approach for the multi-tethered positioning system is to adjust the length of each tether independently using, originally, feedback of readily measurable quantities. Figure 4 shows the tether controller using position

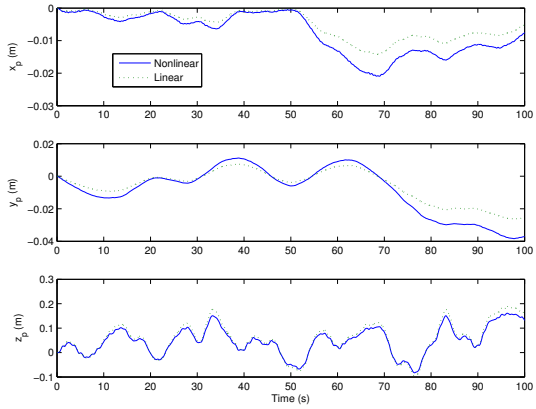

Fig. 3. Comparison of nonlinear and linear simulation results for platform position with no control.

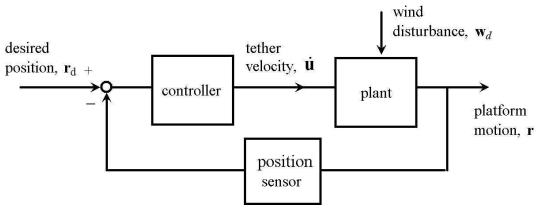

Fig. 4. Block diagram of control system with position feedback.

feedback of the platform. Because of its simplicity for implementation and tuning, a PID controller was investigated first, followed by an optimal LQG approach. Both types of feedback controllers were then augmented by the introduction of a feedforward control term based on the leash forcing function, which is also readily measurable.

3.1 PID Control

The general equation for the PID controller, which specifies the the tether velocity, $\dot{L}_i$, for the i-th tether is as follows:

$$\dot{L}_i = K_D \dot{e}_i + K_P e_i + K_I \int e_i dt \tag{3}$$

where e_i is the instantaneous error of the corresponding tether length and K_D, K_P, and K_I are the derivative, proportional and integral gains respectively. The error for each tether is calculated using:

$$e_i = \|\mathbf{r}_d - \mathbf{r}_{Wi}\| - \|\mathbf{r} - \mathbf{r}_{Wi}\| \tag{4}$$

where $\mathbf{r}$ is the measured position of the payload, $\mathbf{r}_d$ is the desired position and $\mathbf{r}_{Wi}$ is the position of the i-th ground termination or virtual winch. A 2-D representation of the geometry is shown in Figure 5. The idea behind this approach is that the only payload location at which $e_i = 0$ for $i = 1,...,3$ is where $\mathbf{r} = \mathbf{r}_d$. Thus, we can rely on an individual control for each tether, acting together, to bring the payload to its desired location.

Although satisfactory closed-loop performance was observed with the PID controller, its performance is limited by the following three factors: 1) the manually tuned PID gains are sub-optimal, 2) it does not exploit any knowledge of the system dynamics, 3) it uses only position measurements for feedback and does not take advantage of other measured parameters. Therefore, to improve the

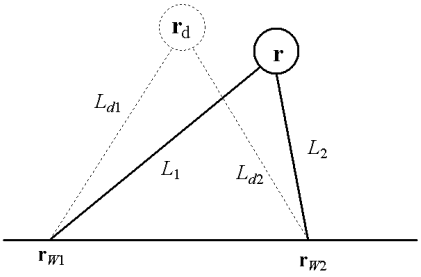

Fig. 5. 2-D representation of tether geometry showing the payload's current position and desired position.

positioning performance of the aerostat system, it is essential to study the potential enhancements of utilizing more advanced control techniques that overcome the major limitations of the PID controller. In this study, both optimal and feedforward control algorithms will be developed and compared to PID results. The control development and testing use a previously developed dynamics model of the system.

3.2 LQG Control

Designing a practical optimal controller is typically a two-stage process where the optimal gain matrix and state estimator or observer are obtained independently. The gain matrix, $\mathbf{K}$ is obtained by solving an algebraic Riccati equation that minimizes the following objective function:

$$J = \int (\mathbf{y}^T \mathbf{Q}\mathbf{y} + \mathbf{u}^T \mathbf{R}\mathbf{u}) dt \tag{5}$$

where $\mathbf{Q}$ and $\mathbf{R}$ are 3×3 weighting matrices corresponding to the output and input respectively. In general, we are concerned more with minimizing the output, which is the platform error, so the elements of $\mathbf{Q} >> \mathbf{R}$ ($\mathbf{Q} = 1 \times 10^6 \mathbf{R}$, where $\mathbf{R}$ is an identity matrix). Matlab's *lqry* function was utilized to solve the ARE and determine $\mathbf{K}$ for our LTI system.

Since $\mathbf{K}$ presumes full-state feedback ($\mathbf{u} = -\mathbf{K}\mathbf{x}$), when realistically only the position of the platform is available for feedback, the remaining states must be estimated using a state observer. An optimal approach to state estimation is achieved using a Kalman filter (KF). Combining a KF with the optimal feedback gain $\mathbf{K}$ is known as the linear quadratic Gaussian (LQG) problem. The term Gaussian refers to the statistical distribution of the plant noise, $\mathbf{n}$ and measurement noise, $\mathbf{v}$ represented in the following description of the system:

$$\begin{aligned} \dot{\mathbf{x}} &= \mathbf{A}\mathbf{x} + \mathbf{B}\mathbf{u} + \mathbf{G}\mathbf{n} \\ \mathbf{y} &= \mathbf{C}\mathbf{x} + \mathbf{v} \end{aligned} \tag{6}$$

The Kalman filter provides an estimate of the state, $\hat{\mathbf{x}}$ and it requires the system matrices $\mathbf{A}$, $\mathbf{B}$, $\mathbf{G}$, and $\mathbf{C}$ as well as the estimated covariance matrices of both $\mathbf{v}$ and $\mathbf{n}$, which are assumed to be zero-mean white Gaussian (ZMWG) processes. In our system, the exogenous input, $\mathbf{w}$, which corresponds to the plant noise of the Kalman filter, is not ZMWG, and therefore it was required to add a shaping filter to the plant model that would color a ZMWG process to give it the general stochastic properties of the input, $\mathbf{w}$, Maybeck [1979]. For specific details of the state estimation and controller development see Lambert [2006]. The covariance of the measurement noise, $\mathbf{n}$, was

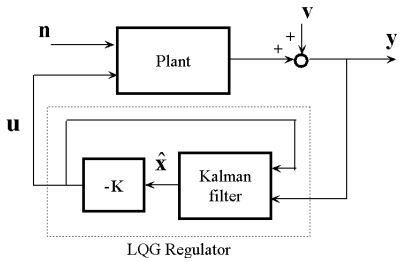

Fig. 6. LQG regulator with Kalman filter state estimation and LQR feedback.

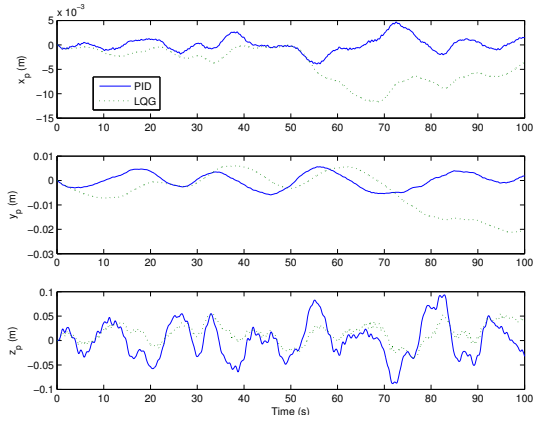

Fig. 7. Comparison of simulation results for platform position using PID and LQG feedback control.

estimated based on observed noise of our DGPS system during static tests, which had a variance of $\sigma^2 = 5\text{mm}^2$. A block diagram showing the LQG controller is given in Figure 6.

Simulation results comparing PID and LQG controllers are given in Figure 7 with the leash forcing function $\mathbf{w}(t)$ obtained during a flight on May 27, 2005. This flight was chosen because the wind speed ($\approx$ 4m/s) was higher than other flights where the control system was activated. The RMS error for the platform position along with the maximum deflection for the two controllers are given in Table 1. Results are also included for the passive system with no controller, and it is observed that even the PID controller offers considerable improvement. The effectiveness of controlled system using both the PID and LQG controller is encouraging considering that the actuators are connected to the platform by flexible tethers several hundred meters in length.

The objective function optimized by the LQG controller minimizes the total error, which in this case is reduced approximately in half compared to what is achieved with PID, despite the fact that the PID controller is slightly more effective in the horizontal x and y-directions. These results are encouraging as it implies that precision of the system can be improved, but it should be mentioned that the LQG controller design presumed perfect knowledge of the plant model and the stochastic properties of the disturbance, while PID control requires no information *a priori*. The robustness of the optimal controller to model and disturbance uncertainties must be analyzed before a comprehensive comparison between controllers can be performed.

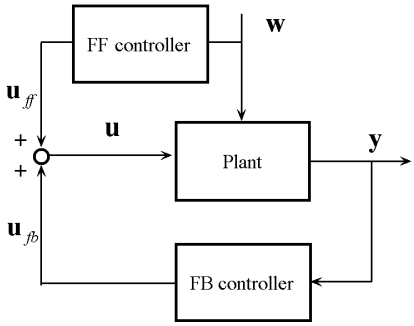

Fig. 8. Block diagram of control system with feedback and feedforward control input.

3.3 Feedforward Control

Recognizing that the vast majority of motion disturbances to the platform are caused by the aerostat's leash, whose tension is a measured quantity in the experimental system, leads us to consider feedforward (FF) control strategies that exploit the knowledge of disturbance force, as shown in Figure 8. Revisiting the LTI model for the system from eq. (2) it becomes apparent that to completely cancel the disturbance, $\mathbf{w}$, the input, $\mathbf{u}$, must satisfy:

$$\mathbf{Bu} = -\mathbf{Gw} \tag{7}$$

Exact cancellation of the disturbance is not possible for our system because of the non-collocation of the actuators and the disturbance force ($\mathbf{B}$ and $\mathbf{G}$ are sparse matrices that give their respective inputs, $\mathbf{u}$ and $\mathbf{w}$, direct influence over different states). Alternatively, this is observed by considering the Moore-Penrose pseudoinverse solution of eq. (7):

$$\mathbf{u} = \mathbf{B}^{+}\mathbf{Gw} \tag{8}$$

where $\mathbf{B}^{+}$ is a left pseudoinverse of $\mathbf{B}$. The Moore-Penrose pseudoinverse yields the trivial solution $\mathbf{u} = \mathbf{0}$. An alternative pseudoinverse can be calculated that gives a non-trivial solution to eq. (8), by coordinating the efforts between the feedforward and feedback control, Friedland [1986].

Expressing the control input $\mathbf{u}$ as the sum of both feedforward and feedback control gives:

$$\mathbf{u} = -\mathbf{K}_{ff}\mathbf{w} - \mathbf{Kx} \tag{9}$$

where $\mathbf{K}_{ff}$ is the feedforward gain given by:

$$\mathbf{K}_{ff} = \mathbf{B}^{+}\mathbf{G} \tag{10}$$

and $\mathbf{K}$ is the feedback gain. This controller development assumes the full-state vector, $\mathbf{x}$, is used for feedback, but when implemented it can use the estimated state $\hat{\mathbf{x}}$.

To solve for $\mathbf{K}_{ff}$ and eventually $\mathbf{B}^{+}$, it is assumed that the feedback gain, $\mathbf{K}$, is already determined (using optimal or other techniques). The development starts by substituting eq. (9) into the state equation.

$$\dot{\mathbf{x}} = (\mathbf{A} - \mathbf{BK})\mathbf{x} - (\mathbf{BK}_{ff} - \mathbf{G})\mathbf{w} \tag{11}$$

The desired controller should attempt to eliminate platform displacement, $\mathbf{y} = \mathbf{Cx} \equiv \mathbf{0}$ and system dynamics $\dot{\mathbf{x}} \equiv \mathbf{0}$. Satisfying both conditions, eq. (11) becomes:

$$\mathbf{C}(\mathbf{A} - \mathbf{BK})^{-1}(\mathbf{BK}_{ff} - \mathbf{G})\mathbf{w} = \mathbf{0} \tag{12}$$

The disturbance $\mathbf{w}$ can be removed from the equation because the controller should be independent of $\mathbf{w}$, resulting in:

$$\mathbf{C}(\mathbf{A} - \mathbf{BK})^{-1}(\mathbf{BK}_{ff} - \mathbf{G}) = \mathbf{0} \tag{13}$$

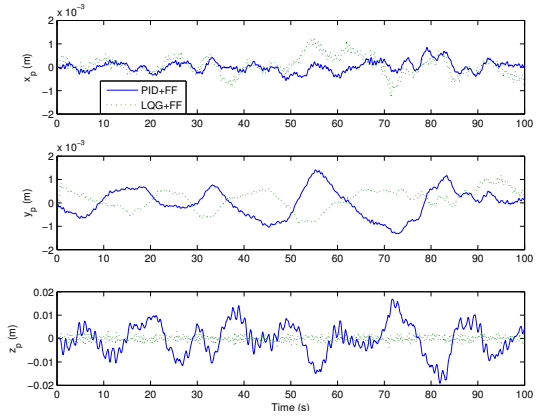

Fig. 9. Comparison of simulation results of platform position for controllers using feedforward and feedback control.

Table 1. Summary of RMS error and maximum displacement (in mm) of the platform for various controllers.

Controller	σ_x	σ_y	σ_z	x_{max}	y_{max}	z_{max}
No control	4.2	9.7	66.1	14.3	26.3	189
PID	1.8	3.3	37.7	5.3	7.7	92.4
PID+FF	0.8	1.1	6.8	2.9	3.3	20.3
LQG	3.4	7.9	19.9	11.7	21.3	57.9
LQG+FF	0.4	0.5	1.7	1.3	1.3	6.7

which can be rewritten as:

$$\mathbf{C}(\mathbf{A} - \mathbf{BK})^{-1}\mathbf{BK}_{ff} = \mathbf{C}(\mathbf{A} - \mathbf{BK})^{-1}\mathbf{G} \tag{14}$$

Finally, the feedforward gain can be solved for by:

$$\mathbf{K}_{ff} = \left[\mathbf{C}(\mathbf{A} - \mathbf{BK})^{-1}\mathbf{B}\right]^{-1}\mathbf{C}(\mathbf{A} - \mathbf{BK})^{-1}\mathbf{G} \tag{15}$$

The collection of terms in front of $\mathbf{G}$ is recognized as a left pseudo-inverse of the input matrix $\mathbf{B}$.

$$\mathbf{B}^{+} = \left[\mathbf{C}(\mathbf{A} - \mathbf{BK})^{-1}\mathbf{B}\right]^{-1}\mathbf{C}(\mathbf{A} - \mathbf{BK})^{-1} \tag{16}$$

It can be shown that the matrix $\mathbf{C}(\mathbf{A} - \mathbf{BK})^{-1}\mathbf{B}$ will possess an inverse if $\mathbf{A}$ is nonsingular and $|\mathbf{CA} - \mathbf{B}| \neq \mathbf{0}$, Friedland [1986]. The specific value of the inverse clearly depends on the feedback gain $\mathbf{K}$, but the existence of an inverse is independent of $\mathbf{K}$.

When designing the LQG feedback controller with state estimation, the Kalman filter must include knowledge of the feedforward control term. This is accomplished by modifying the state-space model originally given by eq.(2) to reflect the changes represented in the state equation of eq.(11).

Results are presented in Figure 9 that compare the performance of feedforward controllers with both LQG and PID feedback. The FF gain, $\mathbf{K}_{ff}$, used for the PID case is calculated following the same procedure as for the LQG case, but because PID does not use full-state feedback and its actual gains can not be easily incorporated into the state equation eq. (11), a suitable full-state feedback matrix, $\mathbf{K}$, was approximated using trial and error. An optimal gain matrix, $\mathbf{K}$, was found by increasing the terms of the matrix $\mathbf{R}$ relative to $\mathbf{Q}$ until the gains matched the general responsiveness of the PID controller. This controller design process is able to produce favorable results, but it is noted that $\mathbf{K}_{ff}$ is calculated from an optimal feedback gain that is obtained heuristically.

The results in Figure 9 show that the PID+FF and LQG+FF produce a similar response in the horizontal directions, but vertically the LQG outperforms the PID by more than a factor of three. A statistical comparison of all four controllers tested in simulation is given in Table 1 . Both feedfoward controllers succeed in limiting the RMS error of the platform to less than 1 cm and the maximum error to less than 3 cm. The exceptional precision obtained with LQG+FF indicates that it should be studied further, as issues related to robustness and model uncertainty were not addressed in this investigation. The PID+FF controller is an attractive option as it is easy to implement and should be less sensitive to model uncertainties. Unfortunately the operational life of our aerostat expired shortly after the test flights conducted in 2005, and the testing program is currently suspended. Therefore it is not currently possible to test these controllers in the field, but because the dynamics model was extensively validated, Lambert et al. [2006a],Lambert [2006], we have confidence in the simulation results presented.

4. CONCLUSION

Control of a multi-tethered aerial positioning system was studied using simulations of a previously validated dynamics model. The effective disturbance-rejection capabilities of the system were demonstrated by PID controller that limited the RMS position error to less than 4 cm. An optimal LQG controller was developed using a linear model of the system and produced about a 50% reduction over the PID controller. Both the LQG and PID feedback controllers were shown to benefit considerably from the addition of a feedforward control term that exploits measurements of the system's main disturbance force. Although the PID + feedforward controller does not perform as well as the LQG + feedforward controller, it limits the RMS error of the platform to less than 1 cm and may be an attractive option due to simplicity and reduced sensitivity to model uncertainty.

ACKNOWLEDGEMENTS

The authors would like to thank the staff at the Dominion Radio Astrophysical Observatory and Dr. Hamid Taghirad of Iran's K.N. Toosi University of Technology for their contributions to this work.

REFERENCES

J.S. Albus, R. Bostelman, and N.G. Dagalakis. The NIST robocrane. *Journal of Robotic Systems*, 10(5):709–724, 1993.

G Barrette and C. Gosselin. Determination of the dynamic workspace of cable-driven planar parallel mechanisms. *Trans. of the ASME Journal of Mechanical Design*, 127: 242–248, 2005.

H. Le Coroller, J. Dejonghe, C. Arpesella, D. Vernet, and A. Labeyrie. Tests with a carlina-type hypertelescope prototype. *Astronomy and Astrophysics*, 426(2):721–728, 2004.

F.R. Driscoll, R.G. Lueck, and M. Nahon. Development and validation of a lumped-mass dynamics model. *Applied Ocean Research*, 22(3):471–485, 2000.

B.Y. Duan. A new design project of the line feed structure for large spherical radio telescope and its nonlinear dynamic analysis. *Mechatronics*, 9(1):53–64, 1999.

J.T. Fitzsimmons, B. Veidt, and P. Dewdney. Steady-state stability analysis of the multi-tethered aerostat platform for the large adaptive reflector telescope. In *Proc. of SPIE International Symposium on Astromical Telescopes and Instrumentation*, pages 476–487, Munich, Germany, March 2000.

B. Friedland. *Control System Design - An Introduction to State-Space Methods*. McGraw-Hill Book Company, 1986.

C. Kossowski and L. Notash. Cat4 (cable actuated truss-4 degrees of freedom): A novel 4 dof cable actuated parallel manipulator. *Journal of Robotic Systems*, 19 (12):605–615, 2002.

C. Lambert. *Dynamics and Control of a Multi-Tethered Aerostat Positioning System*. Ph.d. thesis, McGill University, Montreal, QC, 2006.

C. Lambert, A. Saunders, C. Crawford, and M. Nahon. Design of a one-third scale multi-tethered aerostat system for precise positioning of a radio telescope receiver. In *Canadian Aeronautics and Space Institute Flight Mechanics and Operations Symposium*, Montreal, QC, April 2003.

C. Lambert, M. Nahon, and D. Chalmers. Study of a multi-tethered aerostat system - experimental observations and model validation. *AIAA Journal of Aircraft*, 43(4):1182–1189, 2006a.

C. Lambert, M. Nahon, D. Chalmers, and G. Gilardi. Cable control of an aerostat platform - experimental results and model validation. In *Proc. from the AIAA Guidance, Navigation, and Control Conference and Exhibit*, Keystone, CO, August 2006b.

R.C. Leclaire and C.B. Rice. The local motions of a payload supported by a tritethered natural shape balloon. *US Air Force Report AFCRL-TR-73-0748*, December 1973.

M. A. Masterskikh. A method for holding a pilot balloon or light aerostat at a predetermined height for meteorological observations. *Meteorologiya I Gidrologiya*, 4: 102–104, 1978.

Peter Maybeck. *Stochastic models, estimation and control - Volume 1*. Academic Press, New York, NY, 1979.

M. Nahon. Dynamics and control of a novel radio telescope antenna. In *AIAA Modeling and Simulation Technologies Conference and Exhibit*, pages 214–222, Portland, OR, August 1999.

M. Nahon, G. Gilardi, and C. Lambert. Dynamics and control of a radio telescope receiver supported by a tethered aerostat. *AIAA Journal of Guidance, Control, and Dynamics*, 25(6):1107–1115, 2002.

S.R. Oh, K.K. Mankala, and S.K. Agrawal. Dynamic modeling and robust controller design of a two-stage parallel cable robot. *Multi Body System Dynamics*, 13 (4):385–399, 2005.

R.G. Roberts, T. Graham, and T. Lippit. On the inverse kinematics, statics, and fault tolerance of cable-suspended robots. *Journal of Robotic Systems*, 15(10): 581–597, 1998.

Y.X. Su, C.H. Zheng, and B.Y. Duan. Fuzzy learning tracking of a parallel cable manipulator for the square kilometer array. *Mechatronics*, 15(6):731–746, 2005.